J Comput Neurosci
DOI 10.1007/s10827-006-0012-8

Stability of complex spike timing-dependent plasticity in cerebellar learning

Patrick D. Roberts

Received: 4 April 2006 / Revised: 4 April 2006 / Accepted: 6 November 2006

Abstract Dynamics of spike-timing dependent synaptic plasticity are analyzed for excitatory and inhibitory synapses onto cerebellar Purkinje cells. The purpose of this study is to place theoretical constraints on candidate synaptic learning rules that determine the changes in synaptic efficacy due to pairing complex spikes with presynaptic spikes in parallel fibers and inhibitory interneurons. Constraints are derived for the timing between complex spikes and presynaptic spikes, constraints that result from the stability of the learning dynamics of the learning rule. Potential instabilities in the parallel fiber synaptic learning rule are found to be stabilized by synaptic plasticity at inhibitory synapses if the inhibitory learning rules are stable, and conditions for stability of inhibitory plasticity are given. Combining excitatory with inhibitory plasticity provides a mechanism for minimizing the overall synaptic input. Stable learning rules are shown to be able to sculpt simple-spike patterns by regulating the excitability of neurons in the inferior olive that give rise to climbing fibers.

Keywords Cerebellum · Learning · STDP · Modeling · Vestibular

Understanding how the central nervous system processes temporal information is a prominent challenge facing neuroscience today. Our understanding is particularly poor concerning the connection between synaptic plasticity at the cellular level and the dynamics of actual activity patterns as examined in systems-level studies. The cerebellum offers a unique opportunity to investigate this connection using computational studies because of the anatomical regularity of the cerebellar cortex (Llinás, 1975), and because of compelling evidence for synaptic plasticity at several sites within the cerebellum (Hansel et al., 2001).

The present study addresses the properties of associative depression at parallel fiber synapses onto Purkinje cell dendrites (Ito et al., 1982). Associative depression, referred to as long-term depression (LTD) (Ito, 1989), arises from conjunctive stimulation of parallel fibers and climbing fibers. Each climbing fiber spike produces a strong depolarization of the Purkinje cell dendrites that opens voltage gated Ca^{2+} channels (Llinás and Sugimori, 1980). This inflow of Ca^{2+} has been shown to be essential for the induction of this form of LTD (Ekerot and Kano, 1985; Sakurai, 1989). There is also evidence of non-associative enhancement on the parallel fiber synaptic efficacy when stimulating the parallel fiber alone (Sakurai, 1989). Experiments *in vivo* suggest that this enhancement can reverse the associative depression (Ekerot and Jorntell, 2003).

Theoretical studies (Albus, 1971; Marr, 1969) have suggested that synaptic plasticity could lead to learning at a systems level, but these studies are complicated by the effects of complexities in the circuitry, such as the feedback loop from Purkinje cell output to climbing fiber input. It is therefore difficult to determine what effect, if any, the plasticity that has been observed empirically has on the dynamic processes that take place in the cerebellar cortex. The feedback loop can have an important effect on the stability of learning dynamics, as we show in the present study.

Another important reason for difficulty is that empirical studies of synaptic plasticity in the molecular layer of the cerebellar cortex have been carried out in many different preparations, resulting in conclusions that appear contradictory (Mauk, 1997). There is wide disagreement in the

Action Editor: Nicolas Brunel

P. D. Roberts (✉)
Neurological Sciences Institute, OHSU,
505 N.W. 185th Avenue, Beaverton, OR 97006, USA
e-mail: robertpa@ohsu.edu

literature as to the exact timing relation between the parallel fiber input and climbing fiber response that is required for cerebellar long-term depression (LTD) (Mauk, 1997). Part of this disagreement may be due to the use of very different preparations. Examples include the intact cerebellum (Ito et al., 1982), *in vitro* slice preparations (Crepel and Jaillard, 1991; Hirano, 1991; Ito, 1990; Schreurs and Alkon, 1993; Schreurs et al., 1996), and cultured neurons (Lev-Ram et al., 1995; Linden et al., 1991). The possible range for the timing required to induce LTD has been reported to extend from the complex-spike *preceding* the parallel fiber stimulation by 1.75 sec (Karachot et al., 1994) to the complex-spike *following* the parallel fiber stimulation by 250 msec (Chen and Thompson, 1995).

In spite of this disparity in the timing relations, there seems to be agreement that the induction of LTD requires an elevated concentration of Ca^{2+} in Purkinje cell dendrites in conjunction with binding of glutamate at the parallel fiber synapse (Linden and Connor, 1993) (or release of nitric oxide by a spike in the parallel fibers (Lev-Ram et al., 1995)). The presence of voltage-gated Ca^{2+} channels in Purkinje cell dendrites implies that synaptic plasticity can be very sensitive to the presence of inhibitory input, and the timing relations could be shaped accordingly (Callaway et al., 1995). It has been suggested that Ca^{2+} release from intercellular stores may be the main factor for synaptic change, a mechanism that results in drastically different timing relations (Fiala et al., 1996; Houk and Alford, 1996; Miyata et al., 2000). In addition, inhibitory postsynaptic currents in Purkinje cells also show signs of plasticity (Kano et al., 1992) that enhances inhibition when inhibitory inputs are paired with postsynaptic depolarization. The inhibitory currents also show a non-associative reduction when the neuron is hyperpolarized or in the presence of Ca^{2+} chelators (Kano et al., 1992).

Recent empirical study of parallel fiber synaptic plasticity have revealed that a form of non-associative long-term potentiation (LTP) reverses the LTD caused by pairing parallel-fiber spikes with complex spikes (Lev-Ram et al., 2002; Coesmans et al., 2004). Such reversibility of LTD is essential for the system to avoid saturation of the synaptic strengths by noise. If there were no form of LTP that reversed the effects of complex-spike induced associative LTD, then random climbing fiber activity would depress the system permanently.

Theoretical studies of spike-timing dependent plasticity (STDP) can help to predict the physiological STDP learning rule in Purkinje cells because each STDP learning rule has dynamic consequences that could explain how cerebellar LTD leads to observed systems-level adaptation. A class of STDP learning rules that has well-understood learning dynamics is characterized by an associative depression component and a non-associative potentiation component (Roberts and Bell, 2000; Williams et al., 2003; Rumsey and Abbott, 2004). For this class of STDP learning rules, if the time delay between the EPSP and the LTD interval is too great, instabilities will develop (Roberts, 2000a; Williams et al., 2003) that would be evident in *in vivo* simple-spike recordings. Instabilities would manifests as temporal oscillations in the simple-spike rate, oscillations of a frequency determined by the mismatch between the learning rule and the efficacy of the presynaptic for causing a postsynaptic spike.

While some neuronal systems are well enough understood to justify the construction of detailed compartmental models in which various conductances and their spatial distribution are modeled, the high dimensionality of the parameter space in these models, and their complex dynamics, means that a great amount of preliminary experimental data must be collected before the model can be considered biologically realistic (Traub et al., 1991). This is particularly true of cases when a circuit with different types of neurons must be modeled. Although much is known about conductances in cerebellar Purkinje cells, detailed modeling presents formidable computational challenges (DeSchutter and Bower, 1994) that limits testing neuronal behavior on the network level. These difficulties can be partially avoided by subsuming the complexities of the simple spike generation mechanism into a single value that represents the spike threshold of the membrane potential (Abbott and Kepler, 1990). A large class of neuronal models that incorporate such a spike threshold are called *integrate-and-fire* models (Jack et al., 1975; Stein, 1967).

A variation of the integrate-and-fire, the *spike response* model (Gerstner and van Hemmen, 1992), approach uses more realistic representations of postsynaptic potentials (Gerstner, 1998). Typically, the time-course of dendritic integration is assumed *ad hoc* to yield exponential decay with an experimentally derived time constant. On the other hand, if the membrane potential is recorded at the soma, and the spikes are generated near the soma, then a more realistic representation of postsynaptic potentials would be precisely those postsynaptic potentials recorded when presynaptic fibers are stimulated. We represented the neurons of the cerebellum and associated nuclei as spike-response models to evaluate the learning dynamics induced by complex spike-timing dependent plasticity (CSTDP).

In the study reported here, we utilize a mathematical approach that simplifies the task of investigating the effects of different synaptic learning rules. This approach is designed to characterize the network dynamics that result when the exact timing of the pre- and postsynaptic events determine the amount of synaptic change (Roberts and Bell, 2000; Roberts, 2000a; Williams et al., 2003). Our goal is to derive the optimal CSTDP learning rule at Purkinje and stellate cell synapses for stable, systems-level learning. In addition, we show that when plasticity is present at both excitatory and inhibitory synapses, then the synaptic efficacies are minimized

so that the minimum number of synapses are non-zero as recently described (Isope and Barbour, 2002; Brunel et al., 2004).

Mathematical methods

The basic framework of the model was to repeatedly associate (or pair) a climbing fiber spike pattern with a series of adaptable synaptic inputs that represent parallel fiber and inhibitory interneurons. We assumed that the onset of the adaptive synapses was correlated in time with the beginning of the climbing fiber pattern. Specifically, the onset of each adaptable postsynaptic potential (PSP) had a different delay from the beginning of each presentation of the climbing fiber pattern so that the total adaptable input formed a series of overlapping PSPs (Fig. 1(A)). During each parallel-fiber or stellate-cell spike, the synaptic strength (weight) was incrementally changed by a non-associative learning rate. In addition, if a complex spike occurred during an associative window determined by an STDP learning rule, then the synapse was depressed. The model predicted the changes in the simple spike probability of a Purkinje cell during association with complex spike patterns.

Each repetition of paired inputs was parametrized with the variable t representing the evolution of the system during repeated pairings. The time following the beginning of each pairing step denoted by $x_n = n(\Delta x)$ with Δx denoted a time step *during the pairing* and n an integer. Thus, the representation of time in the model has been broken into two components, (x_n, t), where x_n denotes the time following a paired stimulus or motor command, and t represents the number of cycles. If T is the period of the stimulus cycle, then $(x_n + T, t) = (x_n, t + 1)$. These coordinates allow us to separate slow processes from fast processes where t is the slow-process parameter that tracts the influence of synaptic plasticity, and x_n is the fast-process parameter that tracks the neural activity within each stimulus cycle. The model's prediction of the peristimulus histogram has x_n as the independent variable, and the histogram changes as a function of t. The anatomical connectivity represented in Fig. 1(A) identifies the chief elements of the model.

The model neurons were represented as a single compartment spike response model (Gerstner and van Hemmen, 1992). This mathematical approach has been used previously in other systems (Abbott and Blum, 1996; Gerstner et al., 1993; Roberts and Bell, 2000) to evaluate the effects of STDP learning rules. The formalism of spike-response models allows us to complement our simulation studies with analytical results that will provide a deeper theoretical understanding of our predictions. Each model neuron was assigned a time dependent membrane potential, $V(x_n, t)$. This function represented the result of voltage recordings if they were made at the spike-generation zone, and a spike occured whenever the membrane potential of a neuron exceeded a threshold, θ.

The membrane potential was assumed to be influenced by many random processes beyond the control of the investigator. Therefore, we represented the membrane potential as a random variable with a normal (bell-shaped) distribution function. The mean value of the membrane potential is represented by $V(x_n, t)$ with a variance (Levine, 1991) such that

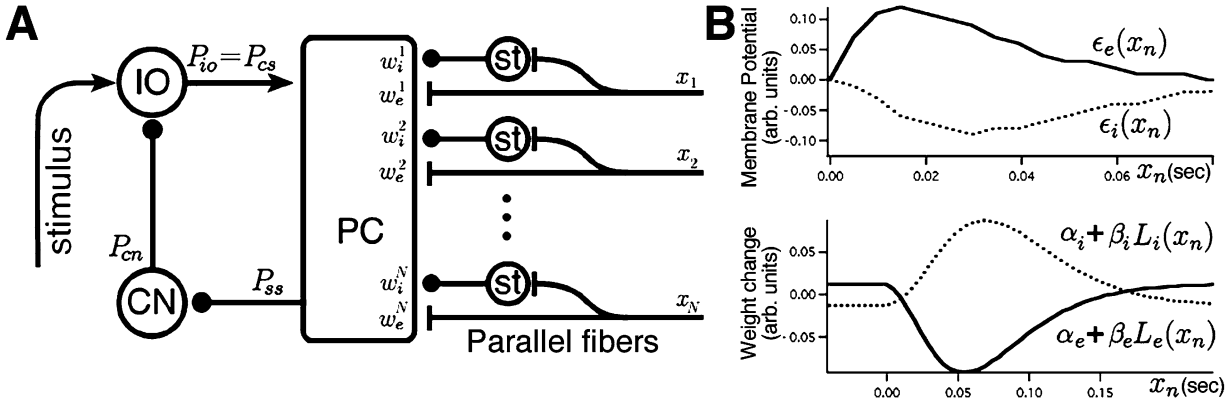

Fig. 1 *Stochastic model of the cerebellum.* (A) The synaptic connectivity of the cerebellum model. The Purkinje cell (PC) simple-spike probability (P_{ss}) is computed from the sum of adaptive inputs from parallel fibers and stellate cells (st). These adaptive inputs are correlated in time with different delays $(x_1, x_2, \ldots, x_N)$ from the beginning of each stimulus presentation. The PC output inhibited a cerebellar target nucleus cell (CN), that inhibited a cell in the inferior olive (IO). The spike probability (P_{io}) was used to generate the complex spike pattern (P_{cs}) that was paired with the spike times of the parallel fiber and stellate cell inputs to apply the STDP learning rule on the synaptic weights $(w_e^1, w_e^2, \ldots, w_e^N$ and $w_i^1, w_i^2, \ldots, w_i^N)$. The model neurons summed their synaptic inputs, plus noise, to generate a spike whenever the total membrane potential reached a threshold. (B) Top panel shows the excitatory parallel-fiber ($\epsilon_e(x_n)$) and inhibitory stellate cell ($\epsilon_i(x_n)$) postsynaptic current multiplied by the synaptic weights in our model Purkinje cell. The bottom panel shows candidate STDP learning rules for the parallel fiber ($\alpha_e + \beta_e L_e(x_n)$, with $\beta_e < 0$) and stellate cell ($\alpha_i + \beta_i L_i(x_n)$, with $\beta_i > 0$) synapse denoting the weight change for a given delay between the onset of the PSP and a complex spike

the activity could be quantified by the spike-probability function, $P(x_n, t) = (1 + \exp(-\mu(V(x_n, t) - \theta)))^{-1}$. The value of the spike-probability function is the probability that a spike will occur during time-step (x_n, t). The function $P(x_n, t)$ has a sigmoid form in V and a value of 1/2 at $V(x_n, t) = \theta$. The mean instantaneous spike frequency could be obtained by dividing the probability function, $P(x_n, t)$, by the absolute refractory period, Δx. Thus, when the membrane potential is high above the threshold, the neuron's output saturates at its maximum frequency, determined by the refractory period.

Adaptive synaptic inputs from parallel fibers and stellate cells contributed to the model neuron's membrane potential linearly through a weighted sum of PSPs. The PSPs were correlated in time with the beginning of each stimulus cycle such that they arrived as a series of delayed synaptic inputs. The use of delay-lines here is intended to approximate the recurrent dynamics of the granule cells interating with Golgi cells to generate correlated parallel fiber spike patterns with respect to mossy fiber stimulations (Buonomano and Mauk, 1994). The delayed inputs generate a *basis set* that can be used to generate a temporal pattern in Purkinje cells with an appropriate adjustment of weighting factors (de Vries and Principe, 1992).

The waveform of each PSP was represented by kernel functions; $\epsilon_e(x_n)$ for excitatory PSPs and $\epsilon_i(x_n)$ for inhibitory PSPs. The kernel functions were fit to Purkinje cell PSPs and $x = 0$ represented the time that the presynaptic spike first reached the synapse (see Fig. 1(B)). The kernels were normalized such that $\sum_n \epsilon_e(x_n) = 1$. The PSP generated by each synaptic input was obtained by multiplying each kernel by a weighting factor, w_e^n for excitatory PSPs and w_i^n for inhibitory PSPs where n denotes the time, x_n, from the beginning of each stimulus cycle when the synapse initiated its PSP. At each time-step in the x-component, up to the limit for temporally correlated adaptive inputs, we associated synapses with an excitatory PSP equal to $w_e^n(t)\epsilon_e(x_m - x_n)$ and an inhibitory PSP equal to $w_i^n(t)\epsilon_i(x_m - x_n)$. The contribution to the average membrane potential, $V_A(x_m, t)$, by the adaptive synaptic inputs in the molecular layer was then computed to be the sum of all PSPs,

$$V_A(x_m, t) = \sum_n w_e^n(t)\epsilon_e(x_m - x_n) + \sum_n w_i^n(t)\epsilon_i(x_m - x_n). \tag{1}$$

where the range of the sum over n represented the limits of temporally correlated input.

The model synapses represent populations of parallel fibers or stellate cells that fire at approximately the same time relative to the associated stimulus. Thus, the synaptic weights, $w_e^n(t)$ and $w_i^n(t)$, combine the presynaptic release probability, the postsynaptic quantal size, and the number of active zones, where the timing of presynaptic spikes are simultaneous within the precision of the model.

The time-dependent activity of Purkinje cells was modeled in accordance with the connectivity represented in Fig. 1. Throughout the stimulus cycle, a delayed sequence of EPSPs was modeled as arriving at the Purkinje cell dendrites. The sequence was temporally correlated to the phase of the stimulation, while uncorrelated units were represented as noise.

The output of a Purkinje cell was represented by two spike probability functions. The first, $P_{ss}(x_n, t)$, quantified the probability of a simple spike, where x_n denoted the phase of the stimulation that began at time $t = 0$. The second spike probability function, $P_{cs}(x_n, t)$, represented the analogous function for the complex-spikes. However, this latter function differs from the corresponding simple-spike probability function in that it does not directly depend on the Purkinje cell's membrane potential. Instead, the complex-spike probability functions depends on the membrane potential of neurons in the inferior olive, such that $P_{cs}(x_n, t) = P_{io}(x_n, t)$ as shown in (Fig. 1(A)).

The simple spike probability function was represented by the sigmoid function of the parallel fiber contribution to the average membrane potential,

$$P_{ss}(x_n, t) = P(V_A(x_n, t)) = \frac{1}{1 + e^{-\mu_{ss}(V_A(x_n,t) - \theta_{ss})}}, \tag{2}$$

where θ_{ss} is the simple spike threshold and μ_{ss} parametrizes the noise in the Purkinje cell.

For the cerebellar STDP learning rule, the dendritic spike that determined synaptic plasticity was represented by the complex-spike (Llinás and Sugimori, 1980). In addition, the PSP time courses were taken from *in vitro* intracellular recordings of Purkinje cells following stimulation of parallel fibers (Neale et al., 2001) (Fig. 1(B)). The average change in synaptic weight per cycle was given by the non-associative weight change minus the average associative change, averaged over the probability of complex spikes (Roberts, 2000a; Williams et al., 2003),

$$\Delta w_e^n(t) = \alpha_e + \sum_m \beta_e L_e(x_m - x_n) P_{cs}(x_m, t). \tag{3}$$

A similar STDP learning rule was used to compute the changes in the inhibitory PSPs, with the inhibitory STDP learning function substituted for the excitatory STDP learning function (Fig. 1(B)).

We have previously developed a method to analyze the stability of a STDP learning rules (Roberts and Bell, 2000; Williams et al., 2003). Whenever a set of adaptive synaptic inputs are correlated in time, and there is a mismatch between

the learning rule $L(x_n)$ and the efficacy of the PSP kernel $\epsilon_e(x_n)$ on dendritic spike generation, then oscillations develop from instabilities in the learning dynamics (in Eq. (3), $L(x_n) = \beta_e L_e(x_n)$). Instabilities result from the synaptic efficacy becoming depressed at a different time relative to the contribution of synapses to the membrane potential. There are no short-term stability issues in this model because the complex spike is too low. To test for long-term, learning instabilities in the learning rule, we compute the Fourier transform of $L(x)$ defined by

$$\mathcal{F}[L](k) = \int dx e^{ikx} L(x). \tag{4}$$

Then, in the continuous limit of t, we find that the condition for stability is

$$\mathrm{Re}\left[\mathcal{F}[L](k)\overline{\mathcal{F}[\epsilon](k)}\right] < 0, \quad k \in (-\infty, \infty), \tag{5}$$

where the overline is the complex conjugate. We represent our postsynaptic potential functions as gamma functions, and their convolutions so that the Fourier transforms that we will need are

$$\epsilon_m(x - x_0) = \frac{(x - x_0)^m}{m!\tau^{m+1}} \exp\left[\frac{-(x - x_0)}{\tau}\right]$$
$$\Rightarrow \mathcal{F}[\epsilon](k) = \frac{e^{-ikx_0}}{(1 - ik\tau)^{m+1}} \tag{6}$$

where $\epsilon_m(x) \equiv 0$ for all $x < 0$, and the function $\epsilon_m(x)$ is normalized such that $\int_0^\infty \epsilon_m(x)dx = 1$. We include x_0 as a temporal-shift parameter in our learning functions to study how timing of the learning window affects stability of the learning dynamics.

The efficacy of parallel fiber synapses on complex spikes is polysynaptic. Thus, in our model, we approximated the efficacy by expanding the spike probability function near a mean spike rate (Roberts, 2004),

$$P_{ss}(x_n, t) = p_{ss} + \mu_{ss} p_{ss}(1 - p_{ss})(V_{ss}(x_n, t) - U_{ss}) + \cdots \tag{7}$$

where p_{ss} is the spontaneous Purkinje cell simple-spike probability during each time-step, and U_{ss} is the background membrane potenial that leads to that rate. The background simple-spike rate is modulated by the parallel fiber and stellate cell spikes that are represented in the time-dependent membrane potential (Eq. (1)), $V_{ss}(x_n, t)$. The linear term in $V_{ss}(x_n, t)$ provides the first-order contribution of the parallel fiber synaptic efficacy in generating a simple spike. A similar expansion for CN cells (Fig. 1(A)) leads to a convolution of PSP functions for each synaptic link given by the CN membrane potential:

$$V_{cn}(x_n, t) = w_{pc\to cn}\epsilon_{cn} * P_{ss}(x_n, t) + w_{pc\to cn}\epsilon_{cn} * P_{cf}(x_n, t)$$
$$\approx w_{pc\to cn}[p_{ss} + \mu_{ss} p_{ss}(1 - p_{ss})\epsilon_{cn} * \epsilon_{pf}(x_{pf}, t)]. \tag{8}$$

where $w_{pc\to cn}$ weights the inhibitory PSP in CN neurons, ϵ_{cn}, caused by Purkinje cell spikes, and x_{pf} is the time of a parallel fiber spike. Since $P_{ss}(x_n, t) \gg P_{cf}(x_n, t)$, we have ignored the second term in our approximation of $V_{cn}(x_n, t)$. In the chain of connections from the parallel fibers to the IO-cells, the efficacy of the parallel fiber spikes on IO neurons is then approximated by $w_{cn\to io} w_{pc\to cn}\mu_{cn} p_{cn}(1 - p_{cn})\mu_{ss} p_{ss}(1 - p_{ss})\epsilon_{io} * \epsilon_{cn} * \epsilon_{pf}(x_{pf}, t)$, where ϵ_{io} is the normalized inhibitory PSP function caused by a CN spike on an IO neuron and $w_{cn\to io}$ is the corresponding synaptic weight. Because the neural spikes are caused by depolarization, the efficacy of synaptic inputs is determined by the timing of the PSPs, rather than simple the presynaptic spike times. Therefore, a delay is embedded in the loop from SS to CS because of the membrane properties of the individual neurons along the pathway.

Our analytic results yielded the equilibrium synaptic weight configuration for large-t, but not the dynamics far from equilibrium. Thus, in order to augment our investigation of the learning dynamics of this model, we developed simulation software based on the spike response model. The studies presented here were based on computer simulation studies using the cerebellar model shown in Fig. 1. We used 200 parallel fibers ($N = 200$) and 200 stellate cells, one Purkinje cell, and one representative from the neural pools in the inferior olive and the cerebellar nucleus. The membrane potential of each postsynaptic cell, $V_{post}(x_m, t)$, was calculated by a sum of the baseline potential, V_0, and PSPs at each time-step, such that $V_{post}(x_m, t) = V_0 + \sum_{n,j} w_j(t)\epsilon_{PSP}(x_m - x_n)S_j^{pre}(x_n)$, where $S_j^{pre}(x_n, t) = 1$ if there were a presynaptic spike at time (x_n, t), and vanishes otherwise. The j-sum was over all presynaptic inputs, and the n-sum was across the stimulus cycle. The PSP kernels, $\epsilon_{PSP}(x_m)$, are shown in Fig. 1(B).

Spikes were assigned by generating pseudorandom numbers drawn from a uniform distribution after calculating the spike probability function, $P(V_{post}(x_n, t))$ (e.g. Eq. (2)). If the random number was less than the spike probability, then a spike was assigned. The parameters in the spike-response models are given in Table 1. A time-step of 5 msec was used in the x-component and periodic boundary conditions were closed at the duration of the stimulus cycle. Each time step in the t-coordinate was counted as a single stimulus cycle. At the end of each stimulus cycle, the complex spike

Table 1 *Model parameters used in simulations*. Cell types refer to Purkinje cells (PC), cerebellar nucleus cells (CN), and inferior olivary cells (IO). All values are normalized so that the synaptic weights are in the range, [0.0, 1.0]. The spike threshold, θ, is given as a percentage of the maximum membrane potential. The maximum membrane potential is the maximum parallel fiber contribution (normalized to unity) plus the maximum baseline potential, $\max(V_0) = 1.0$

Cell type	μ	θ	V_0	α_e	α_i	β_e	β_i
PC	0.3	30%	0.28	0.0012	0.0012	0.18	0.18
CN	0.3	30%	0.40	0	0	0	0
IO	0.2	35%	0.28	0	0	0	0

times were used to adjust the parallel fiber and stellate cell weights through the STDP learning rule (Fig. 2). Java code that generated the figures is available at the authors web site, http://www.ohsu.edu/nsi/faculty/robertpa/lab/java/.

Results

We have evaluated 3 sites of synaptic plasticity for their effects on Purkinje-cell activity: (a) PF to Purkinje-cell synapse, (b) Stellate cell to Purkinje-cell synapses, and (c) the PF to Stellate-cell synapse. In our models, each site of synaptic plasticity was subjected to STDP learning rules, where the direction and magnitude of synaptic plasticity depends on the time difference between pre- and postsynaptic spikes. In these cases, the postsynaptic spike event was the timing of the complex-spike and plasticity induced by pairing presynaptic spikes with complex-spikes was assumed to be reversed by isolated presynaptic spikes. We found conditions for stability of systems-level adaptation at site (a). We also found that synaptic plasticity at site (b) and (c) could stabilize the possible instabilities of the learning dynamics of Purkinje cells, if the learning rule at these synapses are themselves stable.

Optimal stability of CSTDP learning rules

We investigated theoretical constraints on a class of models of cerebellar learning in which the simple-spike rate affects the probability of complex spikes (Ruigrok and Voogd, 1995). The model circuitry assumed that the target nuclei of the cerebellum were inhibited by Purkinje cells and sent projections across the midline to inhibit cells in the inferior olive (Fig. 1). This double inhibition increased the complex spike rate when the Purkinje-cell spike rate increased (Medina and Mauk, 2000). Under these conditions, the exact timing of associative LTD became critical for learning to be stable. Unstable learning dynamics generate oscillations during the stimulus phase (Fig. 3). If the learning dynamics are stable, the learning dynamics cancel modulation of the membrane potential during the stimulus cycle (Buonomano and Mauk, 1994). We tested biologically plausible STDP learning rules (Crepel and Jaillard, 1991; Ito et al., 1982; Lev-Ram et al., 1995; Linden et al., 1991; Schreurs et al., 1996) for stability and found a stable class of STDP learning rules for cerebellar learning, by applying analytic methods to test the stability of STDP learning rules (Roberts and Bell, 2000; Williams et al., 2003). Instabilities appear as oscillatory modes that grow from the fixed point (see Fig. 3(B)). The stability of these modes depends on the sign of real part of the product of Fourier-transformed EPSP and the associative learning function of STDP.

An example of a stable STDP learning rule for a well-characterized system is the adaptive electrosensory processing system of mormyrid electric fish (Bell et al., 1997c; Roberts and Bell, 2000). The STDP learning rule in a cerebellum-like structure, the electrosensory lateral line lobe (Bell et al., 1997a), is based on the opening of postsynaptic NMDA receptors allowing an influx of calcium ions that LTD (Bell et al., 1997c; Han et al., 2000). A non-associative LTP component to the learning rule reverses the LTD (Han et al., 2000). The learning rule is stable because the postsynaptic

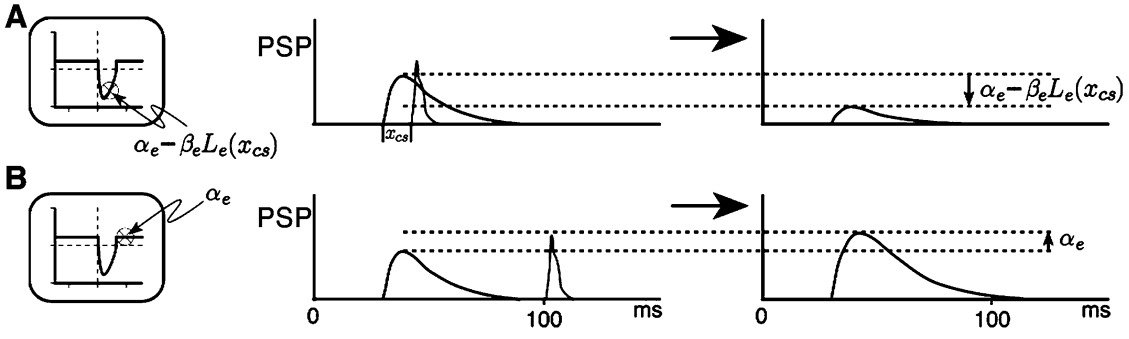

Fig. 2 *Application of learning rule in the simulations*. The STDP learning rule changes the synaptic weights as a function of the exact timing of the complex spike relative to the beginning of the PSP. (A) The learning rule depresses the weight in proportion to $L_e(x_{cs}) = \epsilon_e(x_{cs})$, where x_{cs} is the time of a complex spike, then a complex spike that occurs within the time course of the associative component causes a decrease in the amplitude of the PSP. (B) The synaptic weight is enhanced by a fixed amount, α_e, if the complex spike falls outside the window of depression

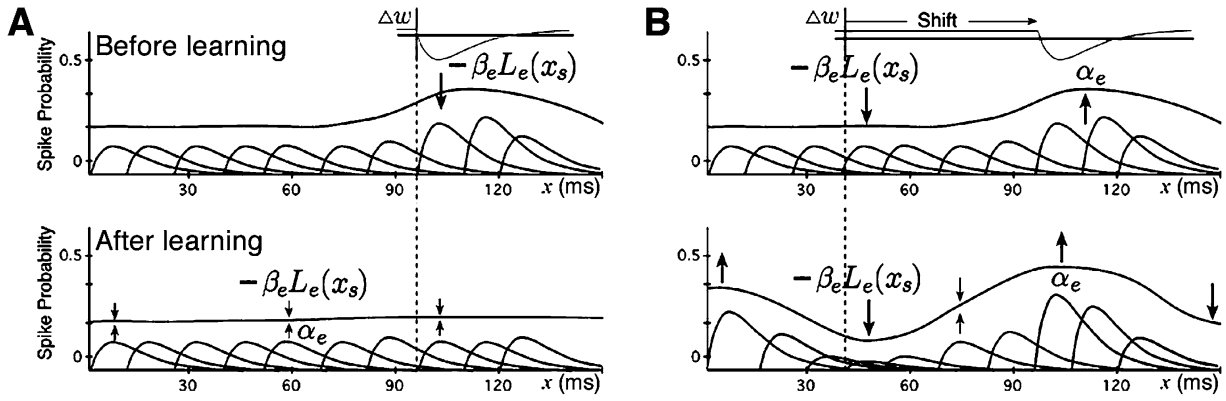

Fig. 3 *Learning instabilities are caused by a mismatched timing of the STDP learning rule*. (A) Example of a stable learning rule where the interval of depression has the same timing as the postsynaptic potentials that lead to dendritic spikes, $L_e(x_{cs}) = \epsilon_e(x_s)$, where x_s is the time of a dendritic spike that leads to depression. A series of excitatory PSPs add together to generate the spikes with a probability shown by the solid line in each graph. Assuming that the efficacy of the PSP input to generate dendritic spikes is the same as the PSP itself, then the stable learning rule will depress the synaptic strength proportionally to the PSPs contribution to the spike probability. The top panel shows several PSPs that are greater than equilibrium late in the cycle ($90 < x < 150$ ms). The depression component of the STDP learning rule dominates in this interval and, after many cycles, these PSPs are reduced to equilibrium (bottom). At equilibrium, the depression due to random dendritic spikes are cancelled by non-associative potentiation, α_e. (B) An unstable learning rule will depress synapses that have not contributed to the above-equilibrium spike probability. A shift in the timing of the depression window is shown here as an example. The PSPs early in the cycle ($x \approx 40$ ms) are depressed by the region of above-equilibrium spike probability late in the cycle ($x \approx 100$ ms). After many cycles the variance grows as oscillations with a frequency determined by the shift on the depression window

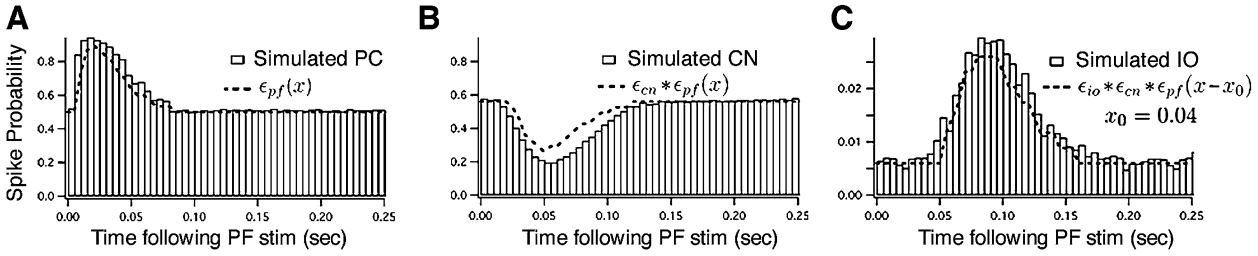

Fig. 4 *Simulated response of model neurons in response to a single parallel fiber spike*. (A) We simulated the spike activity of a Purkinje cell (A), the target cerebellar nucleus (B), and inferior olive neuron (C) that generates the complex spike in the Purkinje cell during a stimulation of the PFs. The spike probability of a target neuron in the inferior olive fits a curve that is a convolution of the 3 postsynaptic potentials in the pathway from the PF to the inferior-olive neuron. The shift is due to synaptic delays in our simulation and nonlinearities introduced by the spike probability function

event is a back-propagating dendritic spike that is generated by parallel fiber EPSP within the same cell. Thus, there is a match between the efficacy of the parallel fiber spikes to generate a postsynaptic event. However, if the same STDP learning rule is applied to the parallel fiber synapse onto Purkinje cells in the cerebellum (Fig. 2), where the postsynaptic event is a complex spike, then the learning dynamics are unstable, as shown in Fig. 5.

In the case of plasticity at the PF synapse onto Purkinje cells, the critical function is the polysynaptic efficacy with which the PF synapse contributes to a complex-spike (Rumsey and Abbott, 2004). We found that the stable STDP learning rule was the convolution of the following 3 functions: the PF-evoked EPSP, the Purkinje-cell-evoked IPSP, and the target nuclei-evoked IPSP in the inferior olive. The shape of these functions is shown in Fig. 4. In the Methods, we discussed an expansion of the spike-probability of neurons in the cerebellar circuit that connects Purkinje cells to the inferior olivary neurons that give rise to climbing fibers. The approximate efficacy of parallel fibers on complex-spikes was found to be proportional to $\epsilon_{io} * \epsilon_{cn} * \epsilon_{pf}(x_n)$. Thus, any stable learning rule is predicted to have an LTD component to its learning rule that satisfies the stability condition (Eq. (5)), yielding the condition on parallel fiber LTD,

$$\mathrm{Re}\left[\mathcal{F}[\beta_{pf} L_{pf}](k)\overline{\mathcal{F}[\epsilon_{io} * \epsilon_{cn} * \epsilon_{pf}](k)}\right] < 0, \quad k \in (-\infty, \infty), \tag{9}$$

We simplify the representations of the postsynaptic potentials to be alpha-functions, $\epsilon_1(x)$ (cf. Eq. (6)), and further let their time constants to be equivalent, $\tau_{pf} = \tau_{cn} = \tau_{io}$. Thus, $\overline{\mathcal{F}[\epsilon_{io} * \epsilon_{cn} * \epsilon_{pf}](k)} = (1 + ik\tau_{pf})^{-4}$, that forces a

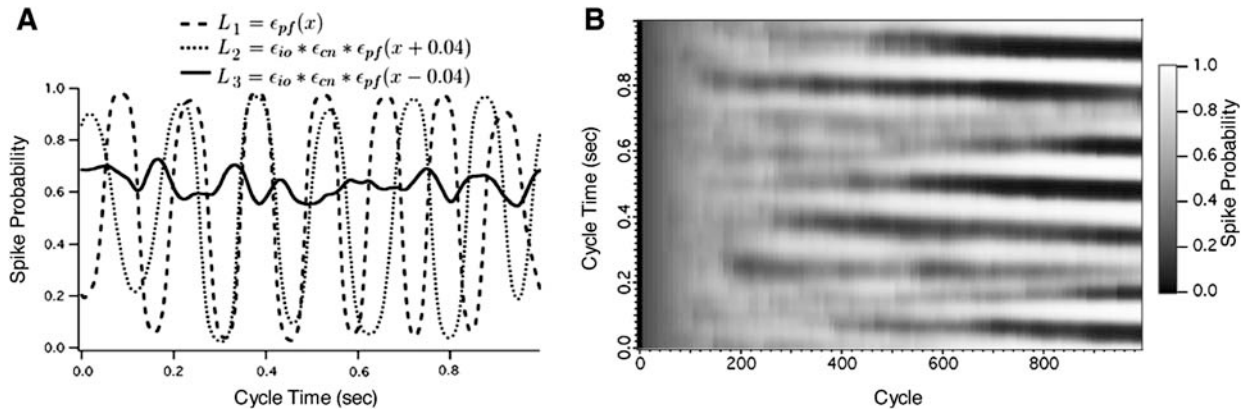

Fig. 5 *Mismatch of STDP learning rule leads to unstable learning dynamics*. (A) The simple-spike probability of the model Purkinje cells shows large oscillations (cycle 1000) for $L_1(x)$, and $L_2(x)$, but nearly stable configuration for the learning rule that matched the efficacy of the parallel fiber synapse on generating complex-spikes, $L_3(x)$. Except for a small range near $x_0 = 40$ ms, the variance of the Purkinje-cell membrane potential is large due to oscillations caused by the learning dynamics. The shift of 40 ms for the stable learning dynamics is required to compensate for the nonlinearities in responses of neurons to the parallel fiber spikes through the chain of synaptic connections from PC → CN →IO (see Fig. 4). (B) The evolution of the PC spike probability shows the growing oscillations caused by the instabilities with $L_1(x)$. Weights are initiated at near, then increase by the non-associative term in the STDP learning rule. After 100 cycles, complex-spikes begin to appear and the increased variance reveals oscillation that grow when the LTD component of the STDP learning rule does not match the complex spike efficacy (Fig. 4(C))

constraint the limits of the time constant for the parallel fiber learning rule satisfying, $\beta_{pf}\mathrm{Re}(1 + k^2\tau_L\tau_{pf} + ik(\tau_L - \tau_{pf}))^4 < 0$. A perfect match between the time-constants of the learning rule and the postsynaptic potential, $(\tau_L = \tau_{pf})$, clearly satisfies the stability condition if $\beta_{pf} < 0$.

We numerically simulated the cerebellar circuit (Fig. 1(A)) using spike-response neuron models to test the analytic prediction of the learning rule. Figure 5 shows the results of the simulation where the change in spike-probability caused by parallel fiber spikes is shown in Fig. 4(A). There is a deviation from our analytic prediction due to the nonlinearities in our spike-probability function (Eq. (2)), forcing a shift in the learning function, $\beta_{pf}L_{pf}(x - x_0)$, where $x_0 = 40$ ms. This shift could have been applied to the inhibitory synaptic learning function with similar results. The simple-spike probability for different learning functions is shown in Fig. 5 showing the oscillations during the cycle caused by instabilities in the learning dynamics. Large oscillations for $x_0 \neq 40$ ms result from a factor of $\exp(-ikx_0)$ in the Fourier transform of $\beta_{pf}L_{pf}(x - x_0)$, a factor that guarantees that there exists a value for k where the stability condition fails.

Effects of CSTDP at the stellate cell synapse onto Purkinje cells

Empirical demonstrations of STDP at inhibitory synapses have revealed two classes of learning rules: (1) symmetric with respect to the presynaptic spike (Woodin et al., 2003) or (2) asymmetric with respect to the presynaptic spike so that the learning window is coincident with the IPSP in the postsynaptic neuron (Han et al., 1999; Haas et al., 2004; Bell et al., 1997b). However, neither of these STDP learning rules helped stabilize the learning dynamics because they themselves are unstable. Plasticity at inhibitory synapses was explored in Roberts (2000b), and we have found that STDP at the synapse from stellate-cell interneurons onto Purkinje-like cells help stabilize learning instabilities if the STDP learning rule at the PF synapse onto Purkinje-like cell causes instabilities. However, extending the range of stability only holds if the STDP learning rule at the inhibitory synapse is itself stable.

The STDP learning rule that we tested in our analysis and simulations was dependent on the interval between a stellate-cell spike and a complex-spike in the Purkinje cell. We have found that the condition of stability of CSTDP at excitatory synapses is also the formula for CSTDP at inhibitory synapses. In a recent publication, we derived an *inversion principle* (Williams et al., 2003) where replacing the postsynaptic potential kernel and the CSTDP learning function by their additive inverse leaves the stability condition invariant. Hence, the stable CSTDP learning rule for an inhibitory IPSP is just minus the stable learning rule for the corresponding excitatory EPSP.

Three possibilities exist for the PF and stellate cell CSTDP learning rules yielding stable learning dynamics: (A) the stellate-cell CSTDP learning rule is different from other examples of STDP learning rules at inhibitory synapses, (B) the recent result (Jörntell and Ekerot, 2002) that climbing fiber collaterals in the superficial molecular layer innervate stellate cells, consequently leading to a depression of the PF synapse onto stellate cells due to an association of complex

spikes and stellate spikes, or (C) the stellate-cell learning rule is unstable, but a stable parallel fiber CSTDP learning rule stabilizes the learning dynamics.

If we assume possibility (A), that the stellate-cell STDP rule is tailored to be stable in the cerebellum, then the Purkinje-cell membrane potential can be stabilized by giving the stellate input a stable learning rule, proportional to the efficacy of stellate-cell spikes to generate complex spikes (Williams et al., 2003). The stable learning function is derived as the inverse of the stellate-cell inhibitory postsynaptic potential convolved with the postsynaptic potential in neurons of the cerebellar nuclei and the inferior olive: $L_{st}(x_n) = \epsilon_{io} * \epsilon_{cn} * \epsilon_{st}(x_n)$. The stability condition for parallel fibers alone (Eq. (9)) has a second term due to the stellate contribution to the membrane potential (see Appendix and Roberts, 2000c) so that the full stability condition becomes,

$$\mathrm{Re}\left[\mathcal{F}[\beta_{pf}L_{pf}](k)\overline{\mathcal{F}[\epsilon_{io} * \epsilon_{cn} * \epsilon_{pf}](k)} + \mathcal{F}[\beta_{st}L_{st}](k) \times \overline{\mathcal{F}[\epsilon_{io} * \epsilon_{cn} * \epsilon_{st}](k)}\right] < 0, \quad k \in (-\infty, \infty). \tag{10}$$

If the real part of either term is less than zero, then the combined learning dynamics could still be stable because of the sum of real parts. Our numerical studies found that applying a stable STDP learning rule at the stellate synapse would reduce the oscillations caused by shifts in the parallel fiber learning rule (Fig. 6).

In our simulations, the variance of the membrane potential was not improved with a shift, x_0, near $x_0 = 40$ ms, which was the most stable region of the PF learning rule. These simulations extended the analytic results by showing that, although there are instabilities for most values of x_0, the oscillations are small for delays as large as $x_0 = \pm 50$ ms. This calculation suggests that measuring the CSTDP rule for the parallel fiber synapse alone is not sufficient to determine whether the systems-level learning dynamics are stable. One must also determine the stellate-cell CSTDP learning rule to deduce how the combination of synaptic plasticity at inhibitory synapses combines with plasticity at excitatory synapses.

Possibility (B), that the site of synaptic plasticity for stellate inhibition is at the parallel fiber synapse onto stellate cells was originally suggested by Albus (1971) using the argument that there are far more parallel fiber contacts onto stellate cells than stellate cell contacts onto Purkinje cells. Thus, synaptic plasticity at the parallel fiber synapse onto stellate cells would maximize the storage capacity of the network. Empirical evidence of synaptic plasticity at this synapse has been reported (Jörntell and Ekerot, 2002), but the amount of plasticity for delays between parallel-fiber spikes and complex spikes, ie. the complete CSTDP learning rule, was not determined. Our analytic model suggests that a stable CSTDP learning rule would satisfy the condition:

$$\mathrm{Re}\left[\mathcal{F}[L_{pf\to st}](k)\overline{\mathcal{F}[\epsilon_{io} * \epsilon_{cn} * \epsilon_{st} * \epsilon_{pf\to st}](k)}\right] < 0, \quad k \in (-\infty, \infty), \tag{11}$$

where here $\epsilon_{pf\to st}(x)$ is the EPSP in stellate cells caused by a parallel fiber spike. The added convolution induces a longer delay between the parallel-fiber spike and the climbing-fiber spike than in our previous example.

The third possibility (C) is that the learning dynamics of the parallel fiber synapse onto a Purkinje cell stabilizes the unstable learning dynamics of plasticity of the inhibitory input to Purkinje cells. In this case we refer again to Eq. (10) and conclude that if inhibitory plasticity is unstable, then this places stricter constraints on the parallel-fiber synapse. All three of these possible combinations of synaptic plasticity could be tested by measuring the CSTDP learning rules. The main theoretical point here is that a combination of CSTDP at both inhibitory and excitatory inputs to Purkinje cells yields a wider range of parameter values for stable learning dynamics so that the system is more robust.

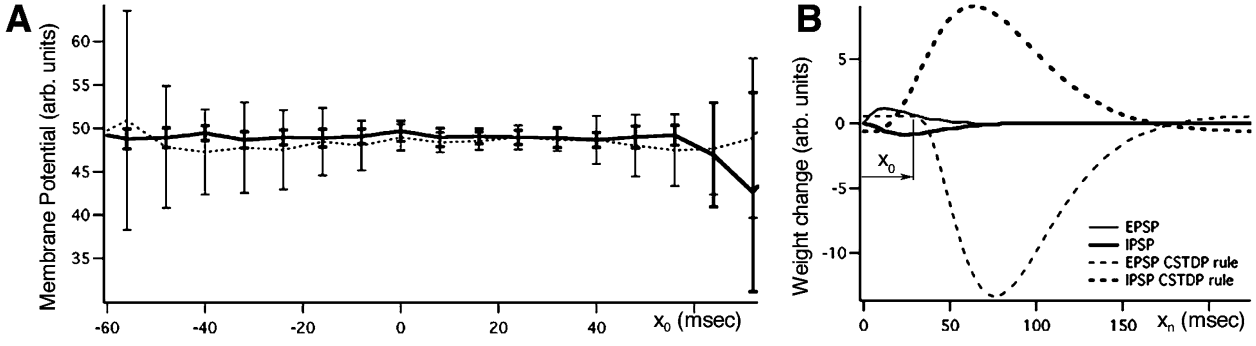

Fig. 6 *Inhibitory CSTDP helps to stabilize the learning dynamics of the PF to Purkinje-cell synapse*. (A) The window of LTD for the CSTDP learning rule at the parallel fiber synapse was shifted for delays $x_0 = -60 \rightarrow 60$ msec. The variance of the membrane is a measure of the instabilities caused by unstable CSTDP learning rules (thin, dotted trace). When a stable CSTDP learning is applied at inhibitory synapses (heavy, solid trace), the instabilities are suppressed. (B) Postsynaptic potential functions and associated CSTDP learning rules for parallel fiber (thin traces) and stellate cell (heavy traces) synapses

Sculpting simple-spike activity with complex-spike response modulation

The learning dynamics of stable STDP learning rules leads to a constant output when parallel fiber inputs are correlated in time. The fixed-point of the output rate is very robust (Roberts and Bell, 2000; Williams et al., 2003) and tends to cancel any modulation of the Purkinje cell rate that is correlated with the parallel fiber spike pattern. However, simple-spikes rates have been observed to be modulated by sensory stimuli or motor activity. Thus, the question arises: How can the Purkinje cell activity be trained for a desired output pattern by the CSTDP learning rule?

Since complex spikes arise in a nucleus separate from the cerebellar cortex, the possibility of external control of the complex-spike patterns can be used to sculpt the simple-spike pattern that is context specific to the stimuli that excite granule cells. This phenomenon of independently controlling dendritic spikes and axonal spike, where the dendritic spikes control synaptic plasticity, has been observed in a cerebellum-like structure (Mohr et al., 2002). The cerebellum appears to be well designed to implement the principle that the activity of one set of inputs (climbing fibers) controls the response of Purkinje cells to another set of inputs (mossy fibers).

In our model circuit (Fig. 1), we modulated the activity of the model neuron representing an olivary cell with a sinusoidal stimulus, $s(x_n)$, that was correlated with the cycle of parallel-fiber delays, $s(x_n) = A\sin(-2\pi x_n/T)$, where $T = 1$ sec is the period of the cycle. The response of the simulated complex spikes is shown in Fig. 7(A) where there is a peak in complex-spike histogram before adaptation takes place. After 1500 cycles (Fig. 7(B)), the modulation of the complex spikes has been cancelled by the simple spike modulation, where the dip in the simple-spike histogram corresponds to a release of the cerebellar nuclei neurons from inhibition, leading to an increase of inhibition of the inferior olive neuron.

The phase relation between the simple-spikes and the complex-spikes is consistent with data from the uvula-nodulus (Barmack and Shojaku, 1995). Although the simulation did not include details of climbing fiber spike generation, it does suggest the following hypothesis: the antiphase relation involves associative depression of the synaptic efficacy in the molecular layer. If the mossy fiber inputs that activate granule cells are temporally correlated with respect to the phase of the stimulus, then those parallel fiber synapse that are coincident with climbing fiber activity will be selectively depressed. The consequence is that during the part of the stimulus when the probability of a climbing fiber response is greatest, the Purkinje cell dendrites receive proportionally less postsynaptic input from parallel fibers, thus reducing the simple spike frequency.

A feature of the learning dynamics that can reduce the overall synaptic input is that the synaptic weights of both excitatory and inhibitory inputs drift in unison if the learning rates are not perfectly matched (Roberts, 2000c). Under these circumstances, the sum of excitatory and inhibitory postsynaptic potentials is constant, but there is an overall depression (of potentiation) that drives the synaptic efficacies to their minimum (or maximum) necessary to reach the fixed point of the learning dynamics. The conditions that minimize the overall synaptic input are that the ratio of the excitatory learning rates are less than the inhibitory learning rates, $\alpha_{pf}/\beta_{pf} < \alpha_{st}/\beta_{st}$. The result shown in Fig. 7(B) is such a case, and many of the synaptic weights, both excitatory and inhibitory, vanish. These learning dynamics suggest a mechanism for the observation that most parallel fiber synapses onto Purkinje cells are silent (Isope et al., 2002).

If the inequality of learning rates is great enough, then the fixed-point of a constant complex-spike rate may be distorted due to saturation of the weights, and the "pressure" of the learning dynamics. An example where α_{st} is large is shown in Fig. 8. Here the non-associative depression of the inhibitory synapses overwhelms the learning dynamics so that the system settles with an increased simple-spike rate during the first phase of the cycle. The average weight configuration (Fig. 8(B)) reveals that the contribution of the synaptic inputs are large only during those phases of the cycle where they increase or decrease the simple-spike rate from its mean output. A striking feature of this numerical simulation is that the CS rate is not constant. The shape of the CS probability is not predicted by the analysis because our analytic methods do not apply when the weights are

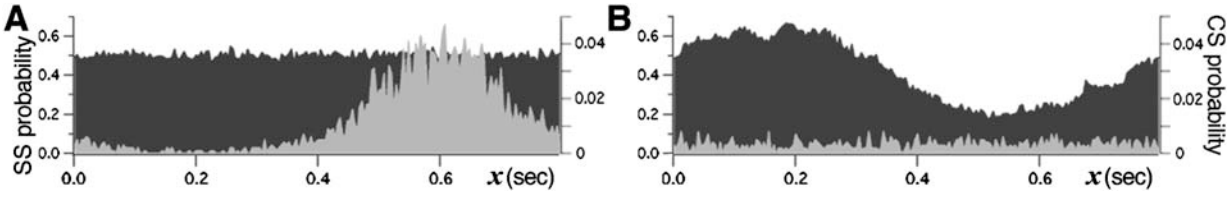

Fig. 7 *Complex-spike pattern sculpts simple spike pattern*. (A) Simulation of network in Fig. 1(A) without synaptic plasticity (histogram of 1000 cycles). Sinusoidal modulation (grey) causes a peak in complex-spike probability during second half of cycle, but the simple-spike probability (black) is constant. (B) After 500 cycles of CSTDP at the parallel fiber synapse onto the Purkinje cell, the simple-spike probability (black) is reduced during the phase where the complex spikes were high. The complex spikes (grey) are now at a constant maintenance rate

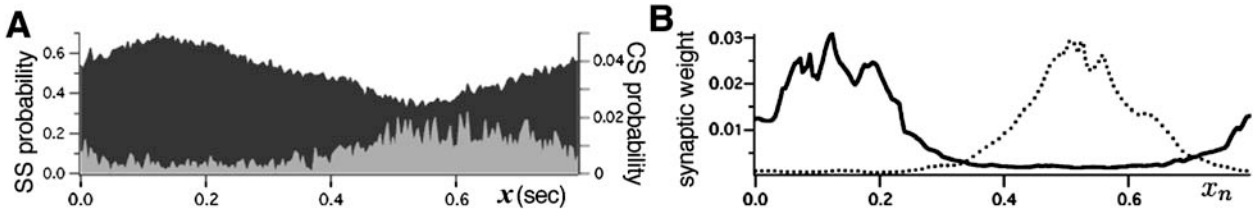

Fig. 8 *Synaptic weight minimization by combining excitatory with inhibitory plasticity*. (A) Simulation of complex spikes (grey) and simple spikes (black) in a single Purkinje cell during oscillatory vestibular stimulation (Barmack, 1995). Result of simulation described in the text showing the same antiphasic response of simple spikes with respect to climbing fiber activity. (B) Average synaptic weights for parallel fibers (solid) and stellate cells (broken) onto model Purkinje cell during sample time where data was take in (A), where x_n labels the beginning of the PSP that is scaled by the weight. Synaptic weights are at their minimum value that generates the spike rates

saturated at a fixed boundary. The numerical results suggest that non-constant spike probability could result if there is a strong non-associative component to the learning rule.

Discussion

In this paper, we derived the learning dynamics of cerebellar Purkinje cells that results from plasticity at synapses onto Purkinje cells. Depression of parallel fiber inputs, and potentiation of inhibitory interneuron inputs, was assumed to be caused by repeated pairing with complex spikes and reversed by a non-associative LTP. We showed that if the synaptic inputs are correlated in the temporal domain, then the timing of the LTD window is critical for stable learning. Instabilities would be observable as oscillations in simple-spike histograms where the frequency depends on the mismatch between the CSTDP learning rule and the efficacy of parallel fibers to generate complex spikes (or the efficacy of stellate cells to inhibit complex spikes). The absence of these oscillations strongly constrains candidate CSTDP learning rules to predict that the window of LTD must be delayed to follow the parallel fiber by at least 50 msec and the maximum depression would be at about 100 msec. Some recent experimental findings agree with this range of delays in our prediction for the timing window for the CSTDP learning rules of parallel fibers (Wang et al., 2000).

Our results regarding the timing of cerebellar LTD were consistent with what is known about the mechanisms of associative LTD at the PF synapse onto Purkinje cells. If parallel fiber LTD were dependent on postsynaptic NMDA receptors, then no delay of the learning window, with respect to the PF EPSP could be realized. An unstable learning rule would result because an NMDA-based learning rule takes the form of an alpha-function (Bell et al., 1997c) that we have shown is unstable (Fig. 5). However, the NMDA-based learning rule is stable in the case of the cerebellum-like electrosensory processing structure in mormyrid electric fish (Roberts and Bell, 2000, 2002). Purkinje-like cells in the mormyrid generate their own dendritic spikes, implying that the PF directly affects the dendritic spike probability via an EPSP that matches the learning function (Bell et al., 1997c). As a result, the learning dynamics are stable in the sense that oscillations are not generated within the electric discharge cycle.

In contrast, LTD in the cerebellum is *independent* of postsynaptic NMDA receptors, and this independence leads to a different shape of the LTD window. Metabotropic glutamate receptors in combination with second messengers may delay the processes that cause LTD from pairing with a complex-spike (Houk and Alford, 1996; Doi et al., 2005; Steuber and Willshaw, 2004), possibly taking a form resembling the affect of PF spikes on the complex-spike probability (Fig. 4(C)). The result would be a learning rule that is stable. However, this restriction imposed by stability on the STDP learning rule forbids the possibility of the window of LTD either preceding the PF spike or following the PF spike by more than 80 msec.

The model of cerebellar learning in the present model did not have an explicit representation of mossy fibers spike patterns. Thus, two essential issues were absent from the analysis: (1) how granule cells encode mossy fiber information into parallel fiber activity, and (2) how mossy fiber that project to the cerebellar nuclei affect the dynamics of cerebellar learning dynamics. Although there is considerable theoretical discussion of the first issue in the literature (Albus, 1971; Marr, 1969; Buonomano and Mauk, 1994; Schweighofer et al., 2001), there is little experimental data due to the difficulty of recording from granule cells *in vivo* (Chadderton et al., 2004; Simpson et al., 2005). The present model assumes that the granule cells respond with delays following an sensory or motor event, but this assumption must remain conjectural until further data is available.

The second issue, how mossy fiber collaterals to the cerebellar nuclei affect the dynamics of the system, is partially addressed by the analysis of complex-spike modulation (Figs. 7 and 8). Since the mossy fibers would be carrying the information that is also re-coded by granule cells, possible at delays (Buonomano and Mauk, 1994; Roberts, 2005), then the direct effect would be to reduce the complex-spike response

during the time of the event encoded as mossy-fiber activity. The results following CSTDP would be an increase in simple spike rate that is coincident with the mossy fiber activity. The details would depend on the convergence of mossy fibers and Purkinje cells in the cerebellar nucleus, because these inputs could cancel if there is a balanced convergence.

Another source of dynamics into the systems that is not included in our model is climbing fiber collaterals to cerebellar nuclei. Because of the low rate of climbing fiber spikes, the effects may not be as prominent as mossy fiber collaterals. If the synaptic inputs are particularly strong, then the effect could force a phase shift of the simple spike pattern.

The model does not include an explicit representation of convergence of parallel fibers onto inhibitory interneurons in the molecular layer. The efficacy of parallel fibers onto stellate cells is quite strong and a spike from a single parallel fiber can result in a spike on a stellate cell (Barbour, 1993). One would then expect that few stellate cells deliver only a single spike per stimulus cycle. However, the presence of more spikes per cycle do not affect the qualitative aspects of the results, unless the distribution of spike times is uniform throughout the stimulus cycle. The effectiveness of the inhibitory inputs, in contributing to the final temporal pattern of simple spikes, is increased proportionally to the narrowness of the temporal distribution of the spike timings during the cycle (Roberts, 2005). The present model investigates the extreme case where the stellate cells spike only once per cycle, but that assumption could be softened with similar results as long as each stellate cell spike pattern delivers a different temporal pattern the the Purkinje cell.

The temporal correlation of the parallel fiber spiking activity have been represented by delay-lines in our model. We have assumed that this is an approximation to the actual parallel fiber activity patterns during sensory stimulations. The mechanisms for the delay lines has been numerically explored in the case of eye-blink conditioning (Buonomano and Mauk, 1994), and are possibly due to recurrent interaction of granule cells with inhibitory Golgi cells. There has been a substantial amount of modeling studies to determine the function of Golgi cells. The proposed ideas include: maintaining the parallel fibers in a narrow range of activity in both time and space (Pellionisz and Szentágothai, 1973), causing oscillations in the firing rates of granule cells (Maex and DeSchutter, 1998; Nagano and Ohmi, 1978; Roberts, 1997; Vos et al., 1999), and generating a broader range of timing relative to a sensory stimulus in the parallel fibers than is available in th mossy fiber inputs (Buonomano and Mauk, 1994). However, the recordings of granule cells (Chadderton et al., 2004) during sensory stimuli have not yet revealed the validity of these hypotheses. Our analytic and numerical methods can be modified to account for the actual parallel fiber spike patterns when they become available, but the conclusion remains valid, that learning dynamics constrain the likely CSTDP learning rule during natural cerebellar function.

Appendix

The purpose of this Appendix is to extend the learning stability criterion of Williams et al. (2003) to the case where a second pool of synaptic inputs has an independent STDP learning function. In the main text (Eq. (10)), we use this result to test the learning stability in the presence of a pool of inhibitory stellate-cell synapses in addition to the parallel fiber synapses. We assume that at each x_n, there exists presynaptic spikes for two types of weights, w_n^e and v_n^i. The e-type synapses have postsynaptic potential $\epsilon_e(x_n)$ and STDP learning rule $L_e(x_n)$, and the i-type synapses have postsynaptic potential $\epsilon_i(x_n)$ and STDP learning rule $L_i(x_n)$. Let the vector of the weights be $\vec{W} = (w_1^e, \ldots, w_N^e, w_1^i, \ldots, w_N^i)^T$, where N is the number of weights and T is the transpose.

The coefficient matrix, $\mathbf{Q}$, of the of the linearized weight dynamics (Eq. (28), Williams et al., 2003)

$$\Delta\langle\vec{W}\rangle = \mathbf{Q}\langle\vec{W}\rangle \tag{12}$$

has the block form:

$$\mathbf{Q} = \begin{pmatrix} Q_{ee} & Q_{ei} \\ Q_{ie} & Q_{ii} \end{pmatrix} \tag{13}$$

As shown in Williams et al. (2003), stability of the learning dynamics depends on the eigenvalues of $\mathbf{Q}$. Each block of $\mathbf{Q}$ is circulant and all circulant matrices are simultaneously diagonalizable by a single coordinate transformation S, so that

$$\begin{pmatrix} S^{-1} & 0 \\ 0 & S^{-1} \end{pmatrix}\mathbf{Q}\begin{pmatrix} S & 0 \\ 0 & S \end{pmatrix} = \begin{pmatrix} S^{-1}Q_{ee}S & S^{-1}Q_{ei}S \\ S^{-1}Q_{ie}S & S^{-1}Q_{ii}S \end{pmatrix} = \begin{pmatrix} \Lambda_{ee} & \Lambda_{ei} \\ \Lambda_{ie} & \Lambda_{ii} \end{pmatrix} = \Lambda_Q, \tag{14}$$

where Λ_{ee} is the diagonal matrix of the eigenvalues, $\Lambda_{ee} = \mathrm{diag}(\lambda_1^{ee}, \ldots, \lambda_N^{ee})$, etc. The eigenvalues are the roots of

$$\det(\Lambda_Q - \lambda I) = (-1)^r \prod_{n=1}^{N} \det \begin{pmatrix} \lambda_n^{ee} - \lambda & \lambda_n^{ei} \\ \lambda_n^{ie} & \lambda_n^{ii} - \lambda \end{pmatrix} \tag{15}$$

where λ_n^{ee} is the nth eigenvalue of Λ_{ee}, and r is the number of row and column interchanges to bring the matrix into the final form. Thus, the roots of $\det(\Lambda_Q - \lambda I)$ are the union of the roots of N quadratics, each of the form,

$\lambda^2 - (\lambda_n^{ee} + \lambda_n^{ii})\lambda + (\lambda_n^{ee}\lambda_n^{ii} - \lambda_n^{ei}\lambda_n^{ie})$. In the limiting case of slow-learning, dense-spacing, and long-period (Williams et al., 2003), we transform to the continuous Fourier transforms of the learning rule and postsynaptic potential, $\lambda_n^{ee} \rightarrow \mathcal{F}[L_e](k)\overline{\mathcal{F}[\epsilon_e](k)}$, with $n \rightarrow k$. The non-zero roots can then be shown to be $\lambda = \mathcal{F}[L_e](k)\overline{\mathcal{F}[\epsilon_e](k)} + \mathcal{F}[L_i](k)\overline{\mathcal{F}[\epsilon_i](k)}$. Thus, the excitatory and inhibitory terms separate in the stability criterion

$$\mathcal{F}[L_e](k)\overline{\mathcal{F}[\epsilon_e](k)} + \mathcal{F}[L_i](k)\overline{\mathcal{F}[\epsilon_i](k)} < 0, \quad \text{for all } k \quad (16)$$

as stated in Eq. (10).

Acknowledgments We would like to thank Dr. Neal Barmack, and the members of Dr. Curtis Bell's lab for insightful discussions. Dr. Alan Williams contributed significantly to the formal results presented in the Appendix. This material is based upon work supported by the National Science Foundation under Grant No. IOB-0445648, and by the National Institute of Mental Health under Grant No. R01-MH60364.

References

Abbott LF, Blum KI (1996) Functional significance of long-term potentiation for sequence learning and prediction. Cerebral Cortex 6: 406–416.

Abbott LF, Kepler TB (1990) Model neurons: From Hodgkin-Huxley to Hopfield. In: Garrido L (ed.) Statistical Mechanics of Neural Networks, Springer-Verlag, Berlin, pp. 5–18.

Albus JS (1971) A theory of cerebellar function. Math. Biosci. 10: 25–61.

Barbour B (1993) Synaptic currents evoked in purkinje cells by stimulating individual granule cells. Neuron 11: 759–769.

Barmack NH, Shojaku H (1995) Vestibular and visual climbing fiber signals evoked in the uvula-nodulus of the rabbit cerebellum by natural stimulation. J. Neurophysiol. 74: 2573–2589.

Bell CC, Bodznick D, Montgomery J, Bastian J (1997a) The generation and subtraction of sensory expectations within cerebellum-like structures. Brain. Beh. Evol. 50(Suppl 1): 17–31.

Bell CC, Han V, Sugawara Y, Grant K (1997b) Direction of change in synaptic efficacy following pairing depends on the temporal relation of presynaptic input and postsynaptic spike during pairing. Soc. Neurosci. Abstr. 23: 1840.

Bell CC, Han V, Sugawara Y, Grant K (1997c) Synaptic plasticity in a cerebellum-like structure depends on temporal order. Nature 387: 278–281.

Brunel N, Hakim V, Isope P, Nadal JP, Barbour B (2004) Optimal information storage and the distribution of synaptic weights: perceptron versus purkinje cell. Neuron 43(5): 745–757.

Buonomano DV, Mauk MD (1994) Neural network model of the cerebellum: Temporal discrimination and the timing of motor responses. Neural Comp. 6: 38–55.

Callaway JC, Lasser-Ross N, Ross WN (1995) Ipsps strongly inhibit climbing fiber-activated $[Ca^{2+}]_i$ increases in the dendrites of cerebellar Purkinje neurons. J. Neurosci. 15: 2777–2787.

Chadderton P, Margrie TW, Hausser M (2004) Integration of quanta in cerebellar granule cells during sensory processing. Nature 428: 856–860.

Chen C, Thompson RF (1995) Temporal specificity of long-term depression in parallel fiber-Purkinje synapses in rat cerebellar slices. Learn. Memory 2: 185–198.

Coesmans M, Weber JT, De Zeeuw CI, Hansel C (2004) Bidirectional parallel fiber plasticity in the cerebellum under climbing fiber control. Neuron 44(4): 691–700.

Crepel F, Jaillard D (1991) Pairing of pre- and postsynaptic activities induces long-term changes in synaptic efficacy *in vitro*. J. Physiol. 432: 123–141.

de Vries B, Principe J (1992) The gamma model—A new neural network for temporal processing. Neural Netw. 5: 565–576.

DeSchutter E, Bower JM (1994) An active membrane model of the cerebellar Purkinje cell: II. Simulation of synaptic responses. J. Neurophysiol. 71: 401–419.

Doi T, Kuroda S, Michikawa T, Kawato M (2005) Inositol 1,4,5-trisphosphate-dependent Ca2+ threshold dynamics detect spike timing in cerebellar purkinje cells. J. Neurosci. 25(4): 950–961.

Ekerot CF, Jorntell H (2003) Parallel fiber receptive fields: a key to understanding cerebellar operation and learning. Cerebellum 2(2): 101–109.

Ekerot CF, Kano M (1985) Long-term depression of parallel fibre synapses following stimulation of climbing fibres. Brain Res. 342: 357–360.

Fiala JC, Grossberg S, Bullock D (1996) Metabotropic glutamate receptor activation in cerebellar Purkinje cells as substrate for adaptive timing of the classically conditioned eye-blink response. J. Neurosci. 16: 3760–3774.

Gerstner W (1998) Spiking neurons. In: Maass W, Bishop CM (eds.) Pulsed Neural Networks, MIT Press, Cambridge, pp. 3–54.

Gerstner W, Ritz R, Leo Hemmen J (1993) Why spikes? Hebbian learning and retrieval of time-resolved excitation patterns. Biol. Cybern. 69: 503–515.

Gerstner W, Leo Hemmen J (1992) Associative memory in a network of 'spiking' neurons. Network 3: 139–164.

Haas JS, Selverston AI, Abarbanel HDI (2004) Spike-timing-dependent plasticity of inhibition in the entorhinal cortex. Soc. Neurosci. Abstr./Online Abstract Viewer. 57: 13.

Han V, Bell CC, Grant K, Sugawara Y (1999) Mormyrid electrosensory lobe in vitro: I. Morphology of cells and circuits. J. Comp. Neurol. 404: 359–374.

Han V, Grant K, Bell CC (2000) Reversible associative depression and nonassociative potentiation at a parallel fiber synapse. Neuron 27: 611–622.

Hansel C, Linden DJ, D'Angelo E (2001) Beyond parallel fiber ltd: the diversity of synaptic and nonsynaptic plasticity in the cerebellum. Nature Neurosci. 4: 467–475.

Hirano T (1991) Differential of pre- and postsynaptic mechanisms for synaptic potentiation and depression between granule cell and a Purkinje cell in rat cerebellar culture. Synapse 7: 321–323.

Houk JC, Alford S (1996) Computational significance of the cerebellar mechanism for synaptic plasticity in Purkinje cells. Beh. Brain Sci. 19: 457–461.

Isope P, Barbour B (2002) Properties of unitary granule cell → purkinje cell synapses in adult rat cerebellar slices. J. Neurosci. 22(22): 9668–9678.

Isope P, Dieudonne S, Barbour B (2002) Temporal organization of activity in the cerebellar cortex: a manifesto for synchrony. Ann. NY Acad. Sci. 978: 164–174.

Ito M (1989) Long-term depression. Ann. Rev. Neurosci. 12: 85–102.

Ito M (1990) Long-term depression in the cerebellum. Seminars Neurosci. 2: 381–390.

Ito M, Sakurai M, Tongroach P (1982) Climbing fibre induced depression of both mossy fiber responsiveness and glutamate sensitivity of cerebellar Purkinje cells. J. Physiol. (London) 5: 275–289.

Jack JJB, Noble D, Tsien RW (1975) Electric Current Flow in Excitable Cells. Clarendon Press, Oxford.

Jörntell H, Ekerot CF (2002) Reciprocal bidirectional plasticity of parallel fiber receptive fields in cerebellar purkinje cells and their afferent interneurons. Neuron 34(5): 797–806.

Kano M, Rexhausen U, Dreessen J, Konnerth A (1992) Synaptic excitation produces a long-lasting rebound potentiation of inhibitory synaptic signals in cerebellar Purkinje cells. Nature 356: 601–604.

Karachot L, Kado RT, Ito M (1994) Stimulus parameters for induction of long-term depression in *in vitro* rat Purkinje cells. Neurosci. Res. 21: 161–168.

Lev-Ram V, Makings LR, Keitz PF, Kao JPY, Tsien RY (1995) Long-term depression in cerebellar Purkinje neurons results from coincidence of nitric oxide and depolarization-induced Ca^{2+} transients. Neuron 15: 407–415.

Lev-Ram V, Wong ST, Storm DR, Tsien RY (2002) A new form of cerebellar long-term potentiation is postsynaptic and depends on nitric oxide but not camp. Proc. Natl. Acad. Sci. USA 99(12): 8389–8393.

Levine MW (1991) The distribution of the intervals between neural impulses in the maintained discharges of retinal ganglion cells. Biol. Cybern. 65: 459–467.

Linden DJ, Dickinson MH, Smeyne M, Connor JA (1991) A long term depression of ampa currents currents in cultured cerebellar Purkinje neurons. Neuron 7: 81–89.

Linden DJ, Connor JA (1993) Cellular mechanisms of long-term depression in the cerebellum. Curr. Op. Neurobiol. 3: 401–406.

Llinás R, Sugimori M (1980) Electrophysiological properties of *in vitro* Purkinje cell dendrites in mammalian cerebellar slices. J. Physiol. (London) 395: 197–213.

Llinás R (1975) The cortex of the cerebellum. Sci. Am. 232: 56–71.

Maex R, DeSchutter E (1998) Synchronization of golgi and granule cell firing in a detailed network model of the cerebellar granule cell layer. J. Neurophysiol. 80: 2521–2537.

Marr D (1969) A theory of cerebellar cortex. J. Physiol. 202: 437–470.

Mauk MD (1997) Roles of cerebellar cortex and nuclei in motor learning: contradictions or clues? Neuron 18: 343–346.

Medina JF, Mauk MD (2000) Computer simulation of cerebellar information processing. Nat. Neurosci. 3(Suppl): 1205–1211.

Miyata M, Finch EA, Khiroug L, Hashimoto K, Hayasaka S, Oda SI, Inouye M, Takagishi Y, Augustine GJ, Kano M (2000) Local calcium release in dendritic spines required for long-term synaptic depression. Neuron 28(1): 233–244.

Mohr C, Roberts PD, Bell CC (2002) Cells of the mormyrid electrosensory lobe: I. Responses to the electric organ corollary discharge and to electrosensory stimuli. J. Neurophysiol. 90: 1193–1210.

Nagano T, Ohmi O (1978) Plausible function of Golgi cells in the cerebellar cortex. Biol Cybern. 29: 75–82.

Neale SA, Garthwaite J, Batchelor AM (2001) mglu1 receptors mediate a post-tetanic depression at parallel fibre-purkinje cell synapses in rat cerebellum. Eur. J. Neurosci. 14(8): 1313–1319.

Pellionisz A, Szentágothai J (1973) Dynamic single unit simulation of a realistic cerebellar network model. Brain Res. 49: 83–99.

Roberts PD (1997) Stochastic recruitment in parallel fiber activity patterns. Beh. Brain Sci. 20: 263–264.

Roberts PD (2000a) Dynamics of temporal learning rules. Phys. Rev. E 62: 4077–4082.

Roberts PD (2000b). Electrosensory response mechanisms in mormyrid electric fish. Neurocomputing 32–33: 243–248.

Roberts PD (2000c) Modeling inhibitory plasticity in the electrosensory system. J. Neurophysiol. 84: 2035–2047.

Roberts PD (2004) Recurrent biological neural networks: The weak and noisy limit. Phys. Rev. E 69: 031910.

Roberts PD (2005) Recurrent neural network generates a basis for sensory image cancellation. Neurocomputing 65–66: 237–242.

Roberts PD, Bell CC (2000) Computational consequences of temporally asymmetric learning rules: II. Sensory image cancellation. J. Comput. Neurosci. 9: 67–83.

Roberts PD, Bell CC (2002) Spike timing dependent synaptic plasticity in biological systems. Biol. Cybern. 87: 392–403.

Ruigrok TJH, Voogd J (1995) Cerebellar influence on olivary excitability in the cat. Euro. J. Neurosci. 7: 679–693.

Rumsey CC, Abbott LF (2004) Equalization of synaptic efficacy by activity- and timing-dependent synaptic plasticity. J. Neurophysiol. 91: 2273–2280.

Sakurai M (1989) Depression and potentiation of parallel fiber-Purkinje cell transmission in *in vitro* cerebellar slices. In: Strata P (ed.) The Olivocerebellar System in Motor Control, Springer-Verlag, Berlin, pp. 221–230.

Schreurs BG, Alkon DL (1993) Rabbit cerebellar slice analysis of long-term depression and its role in classical conditioning. Brain Res. 631: 235–240.

Schreurs BG, Oh MM, Alkon DL (1996) Pairing-specific long-term depression of Purkinje cell excitatory postsynaptic potentials results from a classical conditioning procedure in the rabbit cerebellar slice. J. Neurophysiol. 75: 1051–1060.

Schweighofer N, Doya K, Lay F (2001) Unsupervised learning of granule cell sparse codes enhances cerebellar adaptive control. Neuroscience 103: 35–50.

Simpson JI, Hulscher HC, Sabel-Goedknegt E, Ruigrok TJ (2005) Between in and out: linking morphology and physiology of cerebellar cortical interneurons. Prog. Brain Res. 148: 329–340.

Stein RB (1967) The frequency of nerve action potentials generated by applied currents. Proc. R. Soc. B (London) 167: 613–635.

Steuber V, Willshaw D (2004) A biophysical model of synaptic delay learning and temporal pattern recognition in a cerebellar purkinje cell. J. Comput. Neurosci 17(2): 149–164.

Traub RD, Wong RKS, Miles R, Michelson H (1991) A model of a CA3 hippocampal pyramidal neuron incorporating voltage-clamp data on intrinsic conductances. J. Neurophysiol. 66: 635–650.

Vos BP, Maex R, Volny-Luraghi A, DeSchutter E (1999) Parallel fibers synchronize spontaneous activity in cerebellar golgi cells. J. Neurosci. 19: 464–476.

Wang SS, Denk W, Hausser M (2000) Coincidence detection in single dendritic spines mediated by calcium release. Nat. Neurosci. 3(12): 1266–1273.

Williams A, Roberts PD, Leen TK (2003) Stability of negative-image equilibria in spike-timing-dependent plasticity. Phys. Rev. E 68(2/1): 021923.

Woodin MA, Ganguly K, Poo (2003) Coincident pre- and postsynaptic activity modifies GABAergic synapses by postsynaptic changes in Cl^- transporter activity. Neuron 39: 807–820.